Thermal shock driven fracture in a structured solid: dynamic crack growth and nucleation

A. Trevisan[1], G.P. Borzi[1], N.V. Movchan[2], A.B. Movchan[2], and M. Brun[3]

[1]*EnginSoft S.p.A, Padova, Italy*
[2]*Department of Mathematical Sciences, University of Liverpool, UK*
[3]*Dipartimento di Ingegneria Meccanica, Chimica e dei Materiali, Universitá degli Studi di Cagliari, Italy*

Abstract

In this paper we analyse the propagation of an edge crack into a thermoelastic lattice. The propagation within the micro-structured medium is driven by a periodic thermal shock acting on the boundary of the structure. A non standard numerical simulation has been developed which automatically computes the transient crack advance, embedding into the analysis thermal and inertial effects together with the non-linear evolution of the micro-structure. Velocity of propagation is considered for different critical elongation of the elastic ligaments within the lattice and the results are found to be in agreement with previous analytical predictions based on the dispersion properties of the lattice. Nucleation and coalescence are also detailed.

Keywords: dynamic fracture, dispersion, crack nucleation.

1 Introduction

Dynamic fracture in lattice structures is an important area which has attracted attention of physicists and mathematicians, and a large bulk of literature, both experimental and theoretical, has been published on this topic. In particular, the role of dynamic fracture and crack growth instabilities are

of high interest, as highlighted by the Nature paper [1]. Among important theoretical developments we cite the monograph [10], which proposed a novel approach based on mathematical formulation of the Wiener-Hopf type developed specifically for two-dimensional lattices. This work has also led to an advanced concept of the energy dissipation linked to fracture and waves initiated by broken lattice links at the vertex of the crack. Advanced approach to modelling high-speed cracks in lattices and analysis of effects of hyperelasticity were developed in [4].

The recent work [2] has proposed a semi-analytical approach treating a dynamic crack propagating in the thermo-elastic lattice subjected to thermal shocks. This follows the earlier works [5, 6, 7] who studied the phenomenon of thermal striping, which is linked to the growth of surface breaking thermal cracks, and was motivated by the necessity to assess damage in the cooling contour of nuclear power plants. The asymptotic and numerical study of a surface breaking crack under the transient thermal loading was published in [8]. Analytical model based on the Wiener-Hopf formulation to describe propagation of the Slepyan crack in a non-uniform elastic lattice has been presented in [9].

We note that transient fracture in structured solids is an exceptionally challenging topic, especially in the multi-physics framework, which couples physical fields of different nature. This topic is addressed in the present paper, in the framework of the approach, used in the earlier publication [2]. Thermal shocks occur on the boundary of a structured elastic solid, which in turn supports propagation of a transient crack. The simulation gives the description of the transient regimes as well as instabilities leading to nucleation of micro-cracks.

In the present paper, an industrial grade FEM model has been developed for thermal shock driven fracture, with the emphasis on the crack nucleation in the dynamic regime. The analytical inspiration for this publication comes from the earlier works [2, 5, 6, 7, 8, 3]. The ANSYS code is entirely original, and it fully implements transient fracture algorithm, that involves breakages of bonds in an elastic lattice and resetting local initial conditions and each reloading step. Similar to [2] a comparison is drawn to an averaged steady crack propagation, which has been studied in detail in [9]. An illustration of a dynamic fracture nucleation, obtained from the computation, is given in Fig. 1, where the displacement map is presented around the moving crack, and the nucleated micro-crack is clearly identified. The part (a) of this figure shows a single crack, without a nucleation; in part (b) a small crack nucleates ahead of the main crack; the nucleation progresses by the growth of the small crack, as shown in the part (c); finally two cracks coalesce

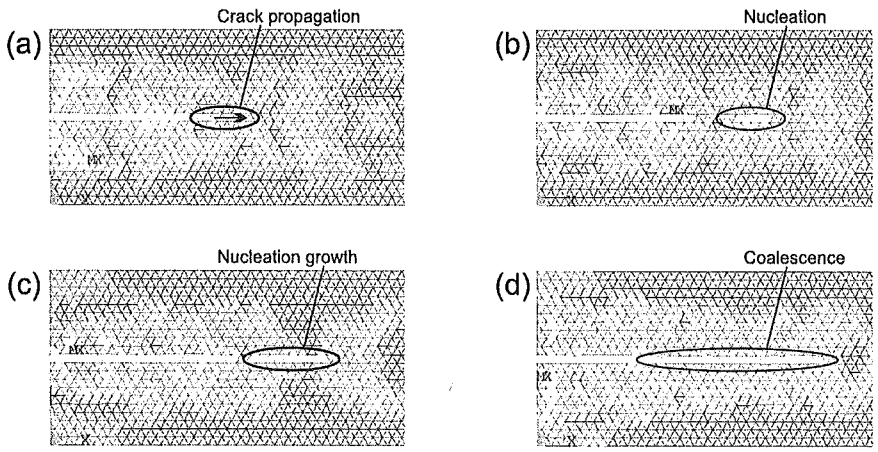

Figure 1: Dynamic crack propagation and nucleation. The normalised radian frequency of the applied load is $\hat{\omega} = \pi/32$, with the relative critical elongation of $\Delta l_t/l = 0.004$. Computational results are presented for the crack advancing dynamically through the lattice: (a) the normalised displacement colour map for an advancing crack prior to a nucleation; (b) the nucleation has occurred - a small secondary crack has been formed ahead of the main crack; (c) the dynamic growth of the secondary crack is observed; (d) coalescence of the main and the secondary crack into a single crack, which continues to propagate dynamically through the lattice.

into a single crack as presented in part (d). The displacement colour map, presented in this figure, also shows a trace of an elastic wave propagating along the crack and interacting with the micro-structure as well as with the nucleation secondary crack. These effects have a significant contribution to the average speed of the crack and to its critical length, as discussed in the main text.

The structure of the manuscript is as follows. Section 2 presents formulation of the problem and introduces main notations. The results of transient simulations of the crack growth are discussed in Section 3. In particular, we highlight comparison with the analytical prediction of the crack growth rate for different loading regimes and lattice parameters and we address nucleation formation and growth. Section 4 describes the computational finite element ANSYS model. Finally, Section 5 presents concluding outline.

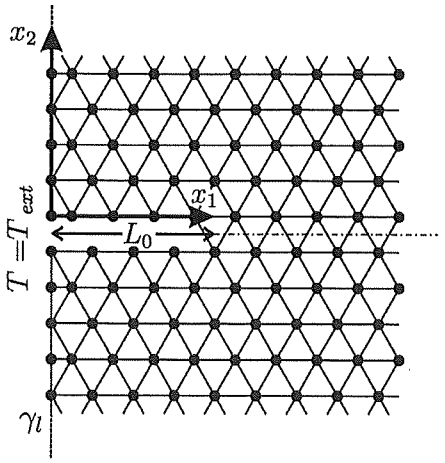

Figure 2: Semi-infinite triangular lattice with a finite edge crack of intial length L_0. The crack grows dynamically and its length L is evaluated as the distance from γ_l to the intersection of the symmetry line (the dashed dotted line) with the first unbroken ligament (centroid).

2 Theoretical background

This study reveals new features of thermally driven fracture that takes into account dynamic effects. A multi-physics formulation includes a parabolic equation for the temperature and a hyperbolic system describing elastic waves. Several dynamic regimes of the thermal crack growth in a lattice structure are identified. Special attention is given to the effect of fracture nucleation during the growth of the crack. The sample geometry is shown in Figure 2, where we depict a triangular elastic lattice occupying a half-plane. Plane strain loading conditions are assumed, and a time periodic distribution of temperature T_{ext} is set on the left boundary γ_l.

A system of short-duration thermal pulses drives an elastic wave away from the boundary, and a fracture criterion, based on the critical elastic elongation of the ligaments is employed in the computations.

The theoretical background for the current formulation has been developed in [2], and the related dynamic analysis of a crack propagating in a discrete infinite lattice was presented in [10, 9]. The continuum model of dynamic thermal crack growth, also known in the literature as "thermal striping", was analysed by [8], while a substantial analysis of thermal striping for the cases of time-periodic thermal loading and non-inertial elastic

solid was published in [5, 6, 7].

In the regimes chosen here, the lattice distribution of the temperature is well-described by the continuum homogenized model, which is analysed in detail in [2].

The time-periodic temperature $T(x_1, t)$ in the half-plane can be evaluated analytically for the continuum case, and the solution in the steady-state regime is given by

$$T(x_1,t) = \sum_{n=-\infty}^{\infty} \frac{iT_0}{2n\pi}(e^{-in\bar{\omega}t} - 1)e^{-\sqrt{\frac{|n\bar{\omega}|}{2\kappa^*}}[1+\mathrm{sgn}(n)i]x_1} e^{in\bar{\omega}t}, \qquad (1)$$

where $\bar{\omega}$ is the radian frequency of the applied load and the other quantities are indicated in eq. (3) and in Table 1.

Rapid variation of the boundary temperature leads to formation of propagating elastic waves away from the boundary. Elastic deformations within the triangular lattice are computed numerically, according to the governing equations:

$$\begin{aligned}\frac{\partial^2 \hat{\mathbf{u}}(\mathbf{p},\hat{t})}{\partial \hat{t}^2} &= \frac{c^2\tau^2}{l^2}\sum_{n=1}^{N(\mathbf{p})}\{\mathbf{a}_n \cdot [\hat{\mathbf{u}}(\mathbf{p}+\mathbf{q}_n,\hat{t}) - \hat{\mathbf{u}}(\mathbf{p},\hat{t})]\mathbf{a}_n\} \\ &+ \frac{c^2\tau^2}{l^2}\hat{\alpha}T_0\sum_{n=1}^{N(\mathbf{p})}\{[\hat{T}(\mathbf{q}_n,\hat{t}) - \hat{T}(\mathbf{p},\hat{t})]\mathbf{a}_n\} \qquad \text{for } \hat{t} > 0, \qquad (2)\end{aligned}$$

where l is the distance between the nearest nodal points, $c = l\sqrt{\mu/m}$, with μ being the stiffness of an elementary ligament and m being the mass placed at nodal points of the triangular lattice. In eq. (2) $\mathbf{u}$ is the displacement, $\mathbf{p}$ a nodal point and $\mathbf{q}_n$ on of the $N(\mathbf{p})$ adjacent nodal point. The other quantities are indicated in eq. (3) and in Table 1.

Here we use the normalized variables (indicated with the "hat" symbol), with the normalization chosen as follows

$$\begin{aligned}&\left(\mathbf{x}, \mathbf{u}, B, H, L_0, L, L^*, \Delta l, \Delta l_t, \tfrac{1}{\xi}\right) = l\left(\hat{\mathbf{x}}, \hat{\mathbf{u}}, \hat{B}, \hat{H}, \hat{L_0}, \hat{L}, \hat{L^*}, \hat{\Delta l}, \hat{\Delta l_t}, \tfrac{1}{\hat{\xi}}\right); \\ &\left(t, \theta, \tfrac{1}{\bar{\omega}}\right) = \tau\left(\hat{t}, \hat{\theta}, \tfrac{1}{\hat{\omega}}\right); \quad v = c\hat{v}; \quad \omega = \tfrac{c}{l}\hat{\omega}; \\ &\left(T, T_c, T_{ref}, \tfrac{1}{\alpha}\right) = T_0\left(\hat{T}, \hat{T_c}, \hat{T}_{ref}, \tfrac{1}{\hat{\alpha}}\right). \qquad (3)\end{aligned}$$

The notation $\bar{\omega}$ is used for the radian frequency of the applied thermal load, i.e. $\bar{\omega} = 2\pi/\theta$, and $\hat{\bar{\omega}} = \tau\bar{\omega} = \frac{2\pi\tau}{\theta}$, where τ stands for the duration of

the thermal pulse, as illustrated in Figure 9. . The system is supplied with the initial conditions:

$$\hat{u}(\mathbf{x},0) = \Phi(\mathbf{x}), \quad \frac{\partial \hat{u}}{\partial t}(\mathbf{x},0) = \Psi(\mathbf{x}), \tag{4}$$

where the choice of functions $\Phi(\mathbf{x})$ and $\Psi(\mathbf{x})$ is defined on every iteration of the transient process, following the evolution of the crack propagation as ligaments of the lattice break. At the start of the numerical procedure, these functions are chosen to be zero.

3 Transient crack growth

Floquet waves in an elastic triangular lattice with the boundary along a half-plane possess well-known dispersion properties, discussed in details in [2], [3], [9]– [13]. In these papers it has been demonstrated that for functional equations of the Wiener-Hopf type, which describe propagation of a semi-infinite crack through an infinite lattice, the kernel function contains all the information about dispersion properties of the Floquet waves that may exist in the corresponding periodic lattice.

Finite Element computations are based on an iterative algorithm which uses a positive parameter Δl_t characterising a critical elastic elongation of a ligament of the triangular lattice: when such critical elongation is exceeded the ligament breaks and is removed from the lattice and a new step is started in the numerical computations. The algorithm corresponds to a fully dynamic transient fracture process in subsonic regime.

3.1 The boundary layer regimes and dynamic fracture implications

In the regimes of the rapid change of the temperature at the boundary, there is a well identified boundary layer, dominated by the temperature fluctuation. In that region, the total deformation is dominated by the thermal term. In turn, the rapid change in temperature leads to a formation of an elastic wave propagating away from the boundary of the half-plane. The crack propagates at a high speed in the small region adjacent to the boundary, and then the crack speed is reduced, while the magnitude of the crack velocity is determined by the applied load which generates an elastic wave.

We note that the normalised frequency $\hat{\omega}$ influences the width of the thermal boundary layer and hence the duration of the transition process when the crack is accelerating and the propagation is not steady. In Figure

4 we show that for $\hat{\omega} = \pi/16$ the boundary layer regime is negligibly small, while for $\hat{\omega} = \pi/32$ and $\hat{\omega} = \pi/64$ the transition boundary layer regime exists in both cases and its duration is different, as can be clearly seen in Figure 5 and Figure 6.

The transient problem, involving a threshold critical elongation, is non-linear. Consequently, the failure criterion based on the evaluation of the critical elongation may not lead to bond breakage during the first iteration and more than one successive cycles may be required before the critical elongation is reached and hence the bond breaks.

3.2 Dynamic crack growth for different durations of periodic pulses

We identify an "average" crack speed, as the crack tip moves sufficiently far away from the thermally loaded boundary. Compared to the propagation in the thermally dominant region adjacent to the boundary, the motion of the crack away from the boundary is driven by elastic waves induced by the thermal shock and the breakages of ligaments of the lattice. In turn, the average crack speed is compared with the analytical findings of [2], [3] and [9]. We also note that in the current computations, the critical elongation criterion is applied to the elastic deformation, rather than the total deformation field used in [2].

3.2.1 Characteristic wave speeds

The dispersion relations for the waves in a triangular lattice, associated to a Mode-I fracture, are well-known (see, for example, [11]):

$$\hat{\omega}_p = \sqrt{3 - \cos(\hat{\xi}/2) - 2\cos\hat{\xi}} \quad \text{(for longitudinal waves)}, \tag{5}$$

$$\hat{\omega}_s = \sqrt{6}\cos(\hat{\xi}/4) \text{(for shear waves, also shown as an "optical" branch)} \tag{6}$$

$$\hat{\omega}_R = \sqrt{3 - \sqrt{3}|\sin(\hat{\xi}/4)|} \quad \text{(for Rayleigh waves)}. \tag{7}$$

The "effective speeds" c_p, c_s, c_R, for the longitudinal, shear and Rayleigh waves in the triangular lattice are given by $c_p = c\sqrt{9/8}, c_s = c\sqrt{3/8}$, $c_R = \frac{c}{2}\sqrt{3-\sqrt{3}}$.

Figure 3, which shows the dispersion curves (5)–(7), gives the valuable information extracted from the kernel function of the Wiener-Hopf equation, characterising a Mode-I propagation of a brittle crack in a triangular linear lattice [11]. Apparently, the roots and poles of the kernel function give the

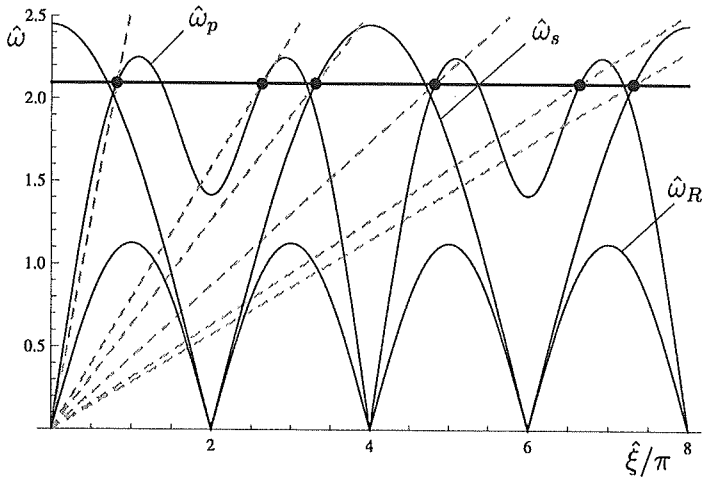

Figure 3: Dispersion diagram for the triangular lattice, with the dispersion curves defined by equations (5)–(7). The rays, connecting the origin to the points of intersection of the line $\hat{\omega} = \text{const}$ with the dispersion curves, show the slope corresponding to admissible crack speeds for Mode-I fracture in the lattice.

curves which are identical to dispersion curves (for the appropriate symmetry modes) in the infinite discrete structure. In particular, for the Mode-I fracture the above figure shows the dispersion curves for the longitudinal waves as well as Rayleigh waves (as a free boundary along the crack is being formed as the crack propagates along the x_1-axis). Understandably, there is also a higher-order mode ("optical" branch in Solid State Physics terms) also representing the shear waves in the homogenised lattice.

The diagram of Figure 3 also gives a valuable information about the waves generated by a propagating crack in the lattice. To do that, we need to choose a slope of a ray, which corresponds to the crack speed, and then look for intersections with the dispersion curves at points corresponding to a positive group velocity. The vertical coordinate of such an intersection point will immediately give the frequency of the wave emanating away from the crack.

The admissible values of average crack speeds $\hat{v}$ for given frequencies have been evaluated according to the method [10]. For the purpose of the illustration, we show these values as slopes of dashed lines in Figure 3. The crack speed is defined by the slope of the rays containing the points of intersection of the lines $\hat{\omega}$ with the parts of the dispersion curves that correspond to positive group velocity. The number of such rays is infinite,

as they are identified by the intersection between the dispersion curves and the horizontal line $\hat{\omega} = \text{const}$, which corresponds to the normalised radian frequency of the forcing temperature T_{ext}.

We note that the critical elongation Δl_t used in this paper as failure criterion is the elastic critical elongation rather than total elongation that includes thermal expansion as well.

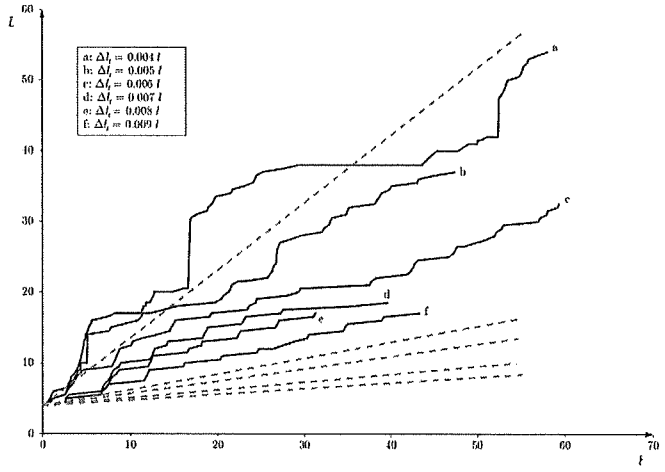

Figure 4: Crack lengths vs. time for $\hat{\omega} = \pi/16$. Different continuous black curves correspond to different critical elongation Δl_t. The slopes of dashed straight lines show the admissible crack speed in the analytical model, solved by the Wiener-Hopf method [11], as illustrated in Figure 3.

Comparative analysis of step-like advance of the crack is presented from Figure 4 to Figure 6, for different duration of the pulse $2\pi/\hat{\omega}$ and for different values of critical elongation Δl_t. The crack tip position as a function of time is shown with solid curves in Figure 4, and these are characterised both by jumps (due to the nucleation and successive merging of voids) and by segments between jumps (corresponding to uniform progression of the crack tip). The slopes of dashed grey lines represent the admissible speeds of the crack propagating through the lattice (as in Figure 3). While Figure 4 was constructed for the case of $\hat{\omega} = \pi/16$, the other Figures 5 and 6 include computations for smaller values of the normalised radian frequency $\hat{\omega} = \pi/32$ and $\hat{\omega} = \pi/64$. As demonstrated in Figure 3, the admissible crack speeds change with the decrease of the frequency, i.e. the steady crack is expected to "slow down" as the value of frequency of the applied external

load decreases.

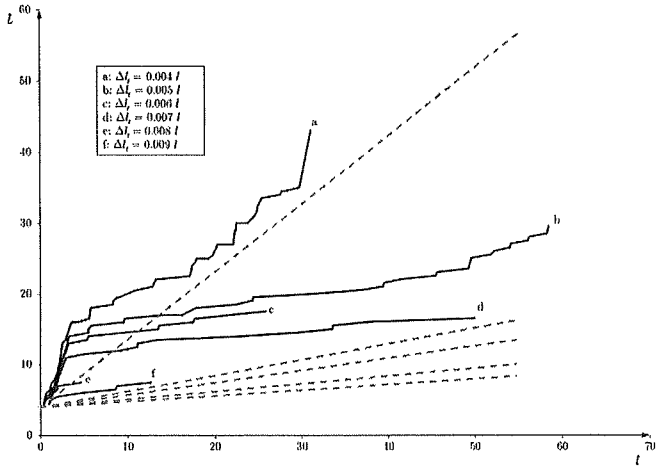

Figure 5: Different continuous black curves correspond to different critical elongation Δl_t. The slopes of dashed straight lines show the admissible crack speed in the analytical model, solved by the Wiener-Hopf method [11].

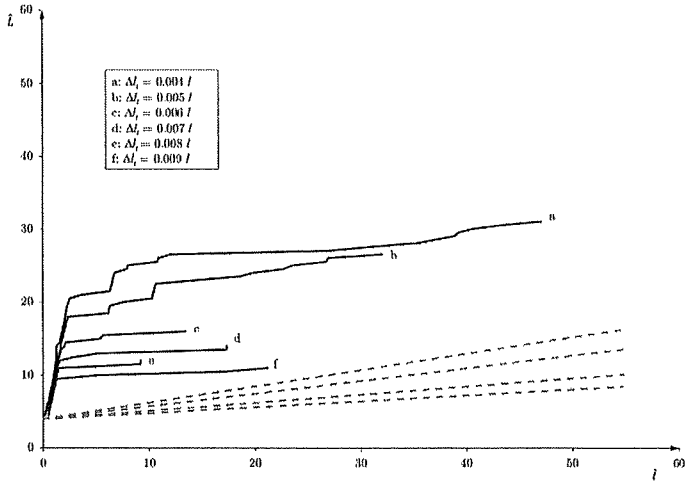

Figure 6: Different continuous black curves correspond to different critical elongation Δl_t. The slopes of dashed straight lines show the admissible crack speed in the analytical model, solved by the Wiener-Hopf method [11].

The solid lines, of stair-like shape, shown in Figures 4-6 show the position of the crack tip as a function of time. It is noted that the crack may accelerate in the region adjacent to the boundary (as in Figures 5, 6), where the thermal boundary layer is important and the stress concentration is high, and then the crack attains a regime, which can be referred to as a steady regime in the context of the averaged crack behaviour. In the non-linear regime, where the failure occurs when a lattice ligament reaches the critical elongation, the crack speed increases when the critical elongation is decreased, while the average speed agrees with one of the admissible crack speeds obtained from the analytical linearised model of a steady crack in a lattice.

For high frequencies, within the stop band, there is no wave propagation and thus there is no energy brought by elastic waves to the crack tip. Hence the crack propagation is suppressed in the high frequency regime.

3.3 Crack nucleation in the lattice

In the earlier papers [2, 5, 6, 7], concerned with the thermal striping phenomenon in elastic lattices, nucleation of the propagating crack was not considered. Nevertheless, crack nucleation was the subject of extensive discussions in other publications [4].

In Figure 1 we show an illustration of a non-linear dynamic crack driven by an external time harmonic load at the normalised radian frequency of $\hat{\tilde{\omega}} = \pi/32$, with the relative critical elongation chosen as $\Delta l_t/l = 0.004$. A small secondary crack is shown to form ahead of the main crack. This process is followed by the growth of the secondary crack and further by the coalescence of the main and of the secondary crack. This leads to the change in the average crack speed as discussed in the text below.

Additional description of the nucleation process is given in Figures 7 and 8. In this case, on each time step where there is a breakage at the crack tip, we note the number of the link that has been broken, which is represented by a dot on the diagrams mentioned. In particular, the length of the crack is defined as the length of the main crack (even in the case when a secondary crack has been formed). Figure 7 presents the evolution of the crack for $\hat{\tilde{\omega}} = \pi/32$, and for critical elongation $\Delta l_t/l = 0.004$. This diagram shows that during the breakage of bonds, nucleation occurs after the 24-th time step. We can also see that this phenomenon persists until crack stops (the right part of the diagram). Further multiple nucleations occur as the crack advances further into the lattice.

In Figure 8, that is representative of the normalised frequency $\hat{\tilde{\omega}} = \pi/32$

and a higher critical elongation $\Delta l_t/l = 0.006$, we can see that nucleation is not present (absence of gaps). This illustration suggests that nucleation is a dynamic phenomenon, strongly dependent on the critical elongation value for bonds of the lattice. In particular, when this critical value increases, i.e. the lattice becomes more resistant to fracture, nucleation disappears. Furthermore, the crack may stop propagating when the resistance of the bonds is sufficiently high.

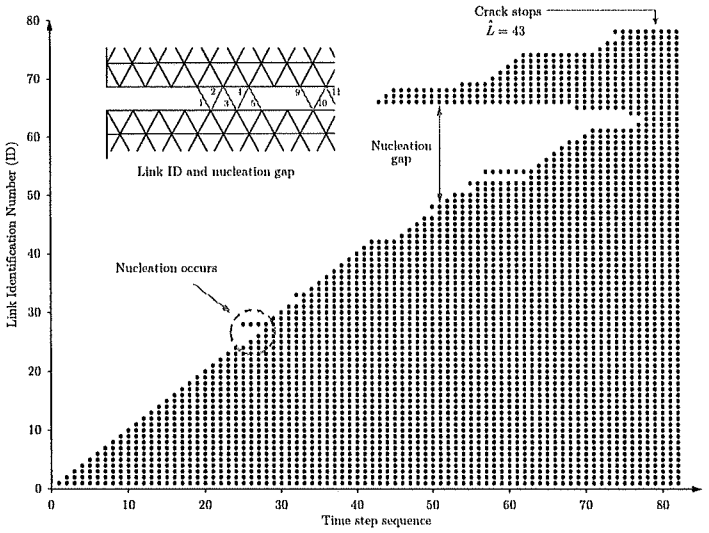

Figure 7: Nucleation diagram for $\hat{\omega} = \pi/32$ duration of the pulse and for critical elongation $\Delta l_t/l = 0.004$. Black dots indicate broken linkages. Nucleation occurs during crack propagation

4 Computational model

4.1 Constants, variables, Units of Measure

In order to implement the numerical model the necessary physical constants and variables have been considered with their associated units of measure, as shown in Table 1. In particular, the International System of Units (SI) has been considered. For temperatures the degree Celsius (°C) has been chosen. Where specified, numerical values have been normalized as described previously (see eq. (3)).

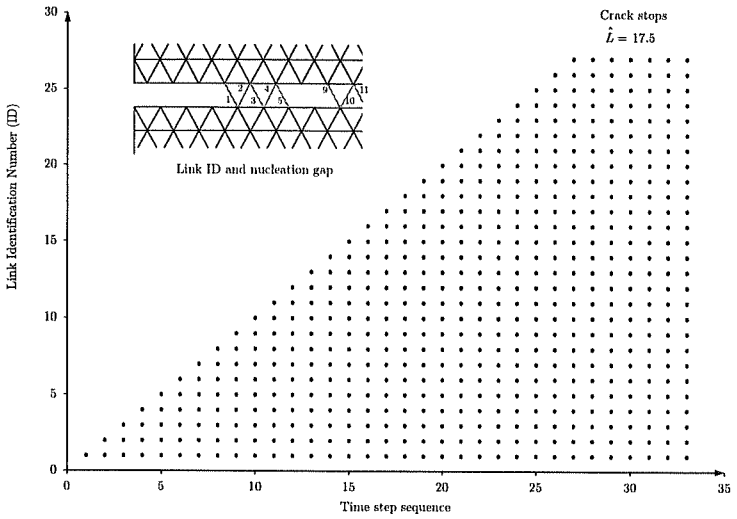

Figure 8: Nucleation diagram for $\hat{\omega} = \pi/32$ duration of the pulse and for critical elongation $\Delta l_t/l = 0.006$. Black dots indicate broken linkages. Nucleation does not occur during crack propagation

The quantity κ^* is the homogenised thermal diffusivity of the continuum, and it is related to the one of the lattice as $\kappa = \kappa^*\sqrt{3}$.

ANSYS was used as FEM computational environment.

4.2 Temperature Function

The temperature imposed on the boundary ($x_1 = 0$) of the lattice is assumed to be uniform in the x_2-direction, and it is represented by a time-periodic series of rectangular pulses as shown in Figure 9:

$$T_{ext}(t) = T_{ext}(0,t) = \sum_{n=0}^{\infty} T_0[H(t - n\theta) - H(t - n\theta - \tau)]. \qquad (8)$$

Here t denotes time, τ is the duration of each pulse, θ is the time interval between two consecutive pulses, $H(\cdot)$ represents the Heaviside step function and T_0 is the maximum value of the applied temperature. It is also assumed that $\theta = 4\tau$. Without loss of generality, the technique discussed here applies to other relations between θ and τ.

l	link length	1	[m]
A	link cross section area	1	[m^2]
μ	link stiffness	1	[N/m]
E	Young modulus	1	[Pa]
ν	Poisson ratio	0.3	
m	node mass	1000	[kg]
α	coefficient of thermal expansion	0.001	[$°C^{-1}$]
κ	lattice thermal diffusivity	1	[m^2/s]
κ^*	continuum thermal diffusivity	$1/\sqrt{3}$	[m^2/s]
L_0	initial crack length	4	[m]
t	time	*variable*	[s]
τ	thermal impulse duration	*variable*	[s]
θ	period of thermal load	*variable*	[s]
T_{ext}	imposed boundary temperature	*variable*	[°C]
T_0	amplitude of imposed temperature	-10	[°C]
l_t	thermal length	1	[m]
Δl_t	critical elongation	*variable*	[m]

Table 1: Constant and variables considered in the numerical problem.

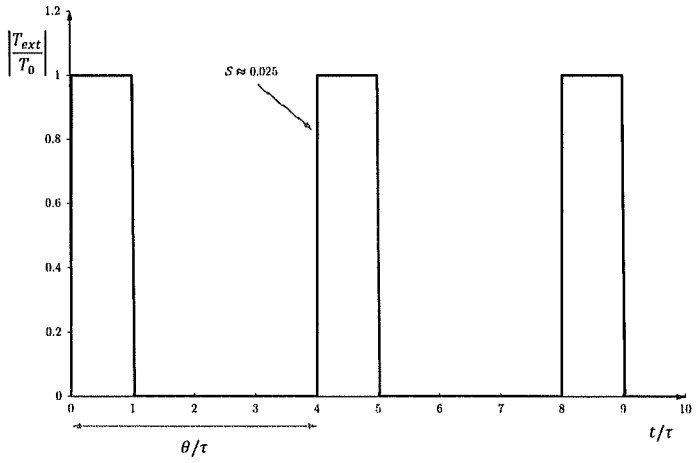

Figure 9: Time variation of the temperature T_{ext} imposed on the boundary γ_l ($x_1 = 0$) of the lattice.

Heat flows through the lattice by means of thermally conducting ligaments. The variation of temperature produces strains (both elastic and thermal) in the ligaments, and stresses. It is important to point out that only elastic strains ε_{el} induce stress and these are used on the iterative procedure to define whether the link is broken or not. The resulting stress field is amplified by the elastic waves generated at the boundary due to the rapid variations in temperature.

The temperature variation in the links is introduced into ANSYS in the form

$$T(x_1,t) = \sum_{n=0}^{\infty} T_0 \left\{ \operatorname{erfc}\left[\frac{x_1}{2\sqrt{\kappa^*(t-n\theta)}}\right] H(t-n\theta) - \operatorname{erfc}\left[\frac{x_1}{2\sqrt{\kappa^*(t-n\theta-\tau)}}\right] H(t-n\theta-\tau) \right\}, \tag{9}$$

which is the solution of the heat conduction problem in a semi-infinite continuum of thermal diffusivity κ^*, with a perfectly thermally-conducting edge crack, exposed to the boundary temperature $T_{ext}(t)$ (eq. (8)) shown in Figure 9. The temperature (9) satisfies the boundary condition given in eq. (8).

The function $T(x_1,t)$ has been implemented within Scilab code and has been evaluated in tabular form in the domain $\mathbb{D}$, where:

$$\mathbb{D} = \{0 \le x_1 \le 80; 0 \le t \le 60\tau\}.$$

The sampling points (x_1,t) have been chosen with a x_1 spacing of 0.1 length units and a time spacing dt= 0.025τ. Convergence studies have been carried out in order to show that 0.025τ is sufficiently small to get accurate results.

The forcing temperature function T_{ext} has been considered for different values of $\hat{\omega}$. Table 2 shows the different values of $\hat{\omega}$ considered in calculations, as well as the respective values of τ and θ.

$\hat{\omega}$	τ [s]	$\theta = 4\tau$ [s]
$\pi/16$	8	32
$\pi/32$	16	64
$\pi/64$	32	128

Table 2: The values of $\hat{\omega}$ and pulse durations considered in calculations.

5 Concluding remarks

Thermal crack propagation in a homogeneous elastic triangular lattice excited by periodic thermal pulses has been studied under the assumption of transient regime. Inertia contribution permits to take into account the effect of elastic waves generated by the steep gradient of the boundary temperature. Three different durations of the pulse of the forcing external temperature were considered.

A numerical 2-D model has been developed with ANSYS finite-element code in order to analyse how an existing crack propagates along a specific crack path in the lattice. The problem is non-linear, so a specific solution routine has been developed to solve the problem for a given configuration and to automatically remove the broken ligaments.

Results are presented for a range of lattice parameters, and the progress was facilitated by the advanced numerical technique implemented in the ANSYS framework; in selected particular cases the results are in accordance with trends highlighted in [2]; additionally, the dynamic nucleation has been simulated here and discussed in the context of the lattice fracture.

In the overall range of duration of the pulse considered, it has been noted that the crack tip does not move uniformly in the lattice structure. Crack acceleration and steady regimes, including nucleation were discussed in detail in connection with the analytic model, which predicts admissible speeds for a Mode-I fracture in the lattice. The average crack propagation speed has been estimated using an analytical model, which assumes that the crack propagates in a straight line with constant speed. Results of the numerical lattice model were compared to the analytical predictions with a good agreement.

The numerical model has proved to be efficient in describing the formation and coalescence of voids inside the lattice, the nucleation phenomenon.

Acknowledgements

M. Brun gratefully acknowledges the support of EU FP7, Grant PIEF-GA-2011-302357-DYNAMETA and of Regione Autonoma della Sardegna Grant LR 7 2010 CRP-27585 M4. A.B. Movchan, N.V. Movchan., G.P. Borzi and A. Trevisan gratefully acknowledge the financial support of the European Community's Seventh Framework Programme under contract number PIAP-GA-2011-286110-INTERCER2.

References

[1] Buehler, M.J., Abraham, F.F., Gao, H. (2003). *Hyperelasticity governs dynamic fracture at a critical length scale*, Nature, **426**, 6963, 141-146.

[2] Carta, G., Jones, I.S., Brun, M., Movchan, N.V., Movchan, A.B. (2013). *Crack propagation induced by thermal shocks in structured media*, International J. of Solids and Structures **50**, 2725-2736.

[3] Colquitt, D.J., Nieves, M.J., Jones, I.S., Movchan, N.V., Movchan, A.B. (2012). *Trapping of a crack advancing through an elastic lattice*, Int. J. Eng. Sci., **61**, 129-141

[4] Gao, H. (2001). *Continuum and atomistic studies of intersonic crack propagation*, J. Mech. Phys. Solids, **49**, 2113-2132.

[5] Jones, I.S. (1999). *The application of a displacement controlled weight function for a single edge cracked plate to thermal fatigue damage assessment*, Eng. Fract. Mech. **62**, 249-266.

[6] Jones, I.S. (2005). *Impulse response model of thermal striping for hollow cylindrical geometries*, Theor. Appl. Fract. Mech. **43**, 77-88.

[7] Jones, I.S. (2006). *Thermal striping fatigue damage in multiple edge-cracked geometries*, Fat. Fract. Eng. Mater. Struct. **29**, 123-134.

[8] Movchan, A.B., Jones, I.S. (2006). *Asymptotic and numerical study of a surface breaking crack subject to a transient thermal loading*, Acta Mech. Sin. **22**, 22-27.

[9] Nieves, M.J., Movchan, A.B., Jones, I.S., Mishuris, G.S. (2013). *Propagation of Slepyan's crack in a non-uniform elastic lattice*, J. Mech. Phys. Solids **61**, 1464-1488.

[10] Slepyan, L.I. (2002). *Models and Phenomena in Fracture Mechanics*, Springer.

[11] Slepyan, L.I. (2001). *Feeding and dissipative waves in fracture and phase transition. III. Triangular-cell lattice.* J. Mech. Phys. Solids, **49**, 2839-2875.

[12] Mishuris, G.S., and Slepyan, L.I. (2014) *Brittle fracture in a periodic structure with internal potential energy*, Proc. R. Soc. **A470**, 20130821.

[13] Ayzenberg-Stepanenko, M.V., Mishuris, G.S., and Slepyan, L.I. (2014) *Brittle fracture in a periodic structure with internal potential energy. Spontaneous crack propagation.* Proc. R. Soc. **A470**, 20140121.